A data-driven model on the thermal transfer mechanism of composite phase change materials

DOI:
10.1016/j.tsep.2024.102486

Document Version
Final published version

Thermal Science and Engineering Progress 50 (2024) 102486

Contents lists available at ScienceDirect

Thermal Science and Engineering Progress

journal homepage: www.sciencedirect.com/journal/thermal-science-and-engineering-progress

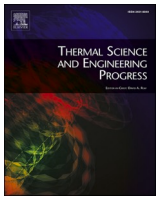

A data-driven model on the thermal transfer mechanism of composite phase change materials

Tan Lo Wong [a], Yasith S. Perera [a], Cristina Vallés [b], Adel Nasser [c], Chamil Abeykoon [a,*]

[a] Northwest Composites Center and Aerospace Research Institute, Department of Materials, Faculty of Science and Engineering, University of Manchester, M139PL, United Kingdom
[b] National Graphene Institute and Henry Royce Institute, Department of Materials, Faculty of Science and Engineering, University of Manchester, M139PL, United Kingdom
[c] Mechanical and Aeronautical Engineering Division L5, Department of Mechanical, Aerospace and Civil Engineering, University of Manchester, M139PL, United Kingdom

ARTICLE INFO

Keywords:
Phase change composites
Maxwell theory
First-principles modeling
Thermal conductivity approximations
Milled carbon fiber

ABSTRACT

Phase change materials (PCMs) that are incorporated with highly conductive nanomaterials to fabricate composite phase change materials (CPCMs), received much focus as a promising energy strategy for latent heat storage and conversion systems, due to their excellent thermophysical properties such as oxidation resistance and large enthalpies of fusion. However, the correct prediction of the thermal conductivity of these CPCMs remains deficient, mainly due to the lack of knowledge on the microscopic heat transfer mechanisms between the nanofiller and matrix interphase. Herein, a data-driven, modified Maxwell model is proposed to determine the thermal conductivity of these CPCMs, using milled carbon fiber (MCF)-reinforced PCMs as validation. This new model incorporates the aspect ratio and morphology smoothness of MCFs and introduces compatibility factors for different types of PCM matrices, which are paraffin and polyethylene glycol (PEG) respectively. At filler loadings above 15 wt%, the theoretical model gave poorer forecasts (with an average prediction error of 0.075) due to the random agglomeration of MCF nanoparticles, which can obstruct the phonon pathway. Regardless, this model accurately estimated the thermal conductivities of MCF/PCMs up to 9 wt% and 11 wt% MCF loading, with percentage fit values being 0.983 and 0.996 for PEG and paraffin systems, respectively. This model also eliminates the limitations of existing models, that were only suitable for composites with low filler loadings (<5 wt%). Hence, this work provides a vital prediction guide for the thermal conductivity of commercial CPCMs.

1. Introduction

The exacerbation of global warming and the escalation of fossil fuel prices have drawn the attention of researchers to smart energy substitutes [1–5]. Composite phase change materials (CPCMs) are excellent candidates for improved thermal efficiency in latent heat energy storage applications [6–10]. CPCMs are intermixtures of conventional phase change materials (PCMs) and highly thermally conductive fillers, such as carbon-based nanomaterials, to achieve enhanced thermal properties, such as thermal diffusivity or degradation stability [11–15]. In addition, CPCMs can also be further encapsulated to prevent the leakage of molten core materials and nanoparticles during phase transitions [16–18].

Despite the excellent thermophysical features possessed by some of these carbon-based nanomaterials such as carbon nanotubes (CNTs), they are very expensive and have other disadvantages such as ineffective dispersion and compromised performance upon being functionalized [19,20]. Therefore, carbon nanofibers (CNFs) emerge as slightly cheaper alternatives as they eliminate the aforementioned limitations of CNTs. While the graphene-based CNTs are arranged as cones or stacked cups as compared to the intact cylinder of a single sheet of graphene in CNT [21,22], CNFs can be appropriately synthesized to reduce the intra-fiber interactions [23]. This is because the lower the Van der Waal's forces within the CNFs, the better the stability when dispersed in polymer matrices [24]. This unique structure of CNFs leads to remarkable thermal and electrical conductivity [25–28].

The thermal conductivity of CNFs usually fluctuates between 4 and 450 W m^{-1} K^{-1}, depending on the length of the high-temperature annealing period used for the fibre synthesizing process [29]. For

* Corresponding author.
E-mail addresses: tanlo.wong@postgrad.manchester.ac.uk, tan.wong@kit.edu (T. Lo Wong), yasith.perera@manchester.ac.uk (Y.S. Perera), cristina.valles@manchester.ac.uk (C. Vallés), a.g.nasser@manchester.ac.uk (A. Nasser), chamil.abeykoon@manchester.ac.uk (C. Abeykoon).

https://doi.org/10.1016/j.tsep.2024.102486
Received 27 June 2023; Received in revised form 8 January 2024; Accepted 26 February 2024
Available online 27 February 2024

instance, by ultrasonic mixing of CNF into paraffin and soy wax, the thermal conductivity increased from 0.32 W m^{-1} K^{-1} (of pristine paraffin) to 0.45 W m^{-1} K^{-1} at 10 wt% of CNFs [30]. The transient temperature response of these CPCMs was substantially improved, without adversely impacting the enthalpy of fusion of paraffin and soy wax, as the loading of CNF increased.

Furthermore, highly conductive carbon fibers (CFs) were incorporated in two ways to enhance the thermal properties of paraffin wax: 1) random orientation of CFs and 2) use of fiber brush [31]. The results showed that the thermal conductivity of CPCMs increased linearly with the volume fraction of the CF brush irrespective of the fiber length. Moreover, the CF brush was useful for facilitating the thermal conduction of packed nanoparticles. Contrastingly, a mere 15 % increase was observed in thermal conductivity upon the addition of CNFs into paraffin [32].

However, the research on the implementation of CNFs as conductive nanofillers for PCMs in thermal storage systems has been limited. This was attributed to the pricey cost of CNFs. One affordable option would be the use of milled carbon fibers (MCFs), which are short-stranded fibrous powder, roughly 100 μm, manufactured from recycled carbon fiber, and are roughly 63 times cheaper than CNFs [33]. Hence, this study explores the use of MCFs to fabricate CPCMs that yield superior heat transfer properties.

Alongside the experimentally measured thermal conductivities of PCM composites, many theoretical models were also established to predict the thermal conductivity of the polymer-based CPCMs. For example, the classical effective medium approximation (EMA) theories and the micromechanics technique made up the two most popular and distinctive types of thermal conductivity calculations. In EMA models [34–44], the polymer-based composites are assumed to be macroscopically heterogeneous, and the low volume fraction of fillers, distant from one another, are also homogenously dispersed. On the other hand, the micromechanics method can be divided into variational principle [45] and the mean field approximations [46,47]. Table 1 summarizes the key outputs of these classical models.

However, these models failed to precisely estimate the thermal properties of composite materials above the percolation threshold. The major difficulty in comprehending the thermal conductivity properties of composite materials is attributed to the lack of knowledge on the fundamental heat transfer mechanisms during phase transitions. In addition to the intrinsic thermal conductivities of the raw materials, as well as the corresponding filler fractions inside the base matrix, CPCMs generally possess a complex network. For instance, the irregular morphologies and dispersion of nanofillers must also be taken into account for the estimation of the overall thermal conductivity. Moreover, the interfacial thermal contact resistance between the filler and matrix interphase also obstructs the heat transfer. This is generally due to 1) localized atomic disorder and acoustic mismatch near the interfacial regions [48], 2) the presence of defects in spherulites of crystalline polymers [49], leading to intense phonon–phonon or phonon-boundary scattering.

Table 1
A summary of classical models' key findings.

Researchers	Model Outputs	Ref.
Maxwell Garnett	Low amounts of spherical particles integrated to the matrix. Thermal interaction between embedded particles were ignored.	35
Hugo Fricke	Filler particles (ellipsoid in shape) dispersed randomly inside the polymer matrix. No experimental verification for the calculation of the average temperature gradient ratio of two phases.	37
Hasselman & Johnson	The influence of particle sizes and interfacial gaps between the fillers and matrix on the thermal diffusivity and conductivity. Applicable for dilute concentrations of dispersions only.	38
Bruggeman & Hanai	The integral embedding principle was employed to calculate the thermal conductivity of multi-component systems, such as nanofluids, aerosols etc., and the effect of thermal interaction was considered. Accurate for high-filler-reinforced composites.	39
Every	Introduced the factor of interfacial thermal resistance between the matrix and the filler particles in particulate composites.	41
Nan	A comprehensive EMA model accounting for the filler loadings, interfacial resistance, orientation, and geometrical distribution and sizes of particles.	44
Mori & Tanaka	An ellipsoidal heterogenic material within an infinitely uniform base matrix subjected to a continuum averaged heat flux. The average internal thermal stress of the matrix and the mean elastic energy of materials with inclusions of transformation strain were analysed. Presence of free interfacial free boundaries addressed.	46

Hence, throughout the last decade, many researchers attempted to improve the theoretical models by introducing other parameters, such as the geometries of particles and interfacial contact resistance. For instance, Xu *et al.* [50] revised the Maxwell model by using the potential mean-field theory in an infinitely-extended heterogenic composite. This approach eliminated the need to include the contributions from far field potentials after the spheres in mesoscale control were removed, hence the effective thermal conductivity can be calculated using linear superposition. The salient feature of this model is the introduction of a contact resistivity fitting parameter that considers the behavior of discrete particles inside a continuous matrix. Yet only composites of low filler fractions, between 0.0 wt% and 0.8 wt% were tested in this study.

In addition, Kim *et al.* [51] modified the Mori-Tanaka model by using the multi-inclusion and multi-phase composite principles, such as computing the thermophysical properties as tensors, namely the number of layers, orientation distributions, shapes, and elastic energies. Hence, this study was able to estimate the isotropic, in-plane, and cross-plane thermal conductivities of polymer composites that possess varying tubular lengths. Yet, the maximum filler loading tested for these carbon-nanotube-reinforced composites was merely 2.5 wt%. Finally, Zhai *et al.* [52] provided a comprehensive review on the effective thermal conductivity of composites, using theoretical and simulation models. It summarized the effects of particles and microstructures on effective thermal conductance, such as complex particle shapes and folded or crooked particles, as well as aggregates, porosity, and connection mechanisms between interphases. The review indicated that most thermal conductivity models only focus on one parameter and lack the inclusion of different factors, hence, they cannot be applied universally.

From the abovementioned model limitations, it is clear that discrepancies exist in experimental CPCM's thermal conductivities. Hence, a generalized model that considered new factors, such as the compatibility between the PCMs and nanofillers, was developed in this study to validify the thermal conductivities of these systems. In addition, the amount of thermally conductive fillers incorporated among phase change materials reported in the existing literature was limited to very low loadings (<5 wt%). Herein, MCFs with increasing range of weight fractions (from 1 wt% to 15 wt%) were added to traditional PCMs, paraffin, and polyethylene glycol (PEG), to improve their thermal performances, via the temperature-assisted solution blending method. To confirm the trends in the thermal conduction of these CPCMs, the thermal conductivities of paraffin/MCF and PEG/MCF samples were then modeled using MATLAB, based on the experimental data. Thus, this work proposed a modified Maxwell model to compute the thermal conductivity of CPCMs, which helps eliminate the shortcomings of other theoretical models.

2. Experimental procedure

2.1. Materials

In this study, paraffin wax and PEG were purchased from Sigma-Aldrich, United Kingdom. MCFs were obtained from Easy Composites

United Kingdom. All materials were used without any additional processing or functionalization. Table 2 captures the price and physical properties of these raw materials.

2.2. Fabrication

The outline of the fabrication of these MCF-reinforced nanocomposites is shown in Fig. 1. The base PCMs were melted from solid to liquid state using a vacuum oven at 120 ℃ for 2 h to ensure that all impurities were removed. Then, the MCF nanofillers were added to different test tubes containing an acetone solution in a room temperature inside the ultrasonic bath. The ratio of nanofiller to acetone was maintained at 1:2, and this excess acetone solution ensured a complete dispersion of the MCFs. The loading fractions were chosen to range from 1 wt% to 15 wt% to prevent significant agglomeration of MCFs, after a series of trial and error. Finally, the molten PCMs and MCFs were combined in multiple beakers and placed in an ultrasonic water bath (Elmasonic P) at 80 ℃ and 37 kHz for 8 h to guarantee thorough mixing between the PCMs and the MCFs, as well as complete evaporation of the excess of acetone. All these samples were immediately cooled in an ice bath to ensure homogeneous solidification and prevent the sinkage of MCF nanofillers due to gravity.

2.3. Characterisation

The morphologies of the samples were scrutinized by Scanning Electron Microscopy (SEM) (Tescan Mira3 SC). The accelerating voltage of 20.0 kV ensured that a sufficient number of electrons could penetrate through the surfaces without damaging the samples to produce clear images of these MCFs-filled CPCMs. A thermometer (Tempos, United States) was used to measure the thermal conductivity and thermal diffusivity of these samples, based on the transient line heat source method, which powered the heat through electric currents to the sensor needles. Finally, a total of 6 measurements per sample were obtained and averaged for the thermal properties, to ensure the reliability and reproducibility of these fabricated samples.

3. Theoretical modelling

To gain further insights into the heat transfer mechanisms in two-phase composites for energy storage applications, several historical models were developed to estimate the thermal conductivity of these composite polymers, as shown in Table 3. These models were theoretical, empirical, and semi-empirical, depending on various factors such as the thermal conductivity of the matrices, the thermal conductivity of the fillers, the morphology of the fillers (shape and size) as well as the added volume of fillers [53].

For instance, the general Maxwell and effective medium theory (EMT) models were the two most widely used models to estimate the thermal conductivity of composite polymers. These two models assumed that fillers are of spherical shape, diffused in a continuously heterogeneous polymer matrix medium, in which the interfacial region between fillers and polymer is smooth [44,54], and these two models are only valid for weight filler fractions below 25 %. The interaction between the filler particles and the effects of particle morphology are ignored.

Table 2
Price and physical properties of materials used in this study.

Name	Properties	Cost (£ per kg)
Paraffin Wax	Melting Point = 53 – 58 ℃	48.4
Polyethylene Glycol (PEG)	Melting Point = 53 – 58 ℃ Bulk Density = 400 – 500 kg m^{-3}	49.5
Milled Carbon Fiber (MCF)	Fiber Length = 100 μm Fiber Diameter = 7.5 μm Fiber Density = 1800 kg m^{-3}	22.75

Furthermore, the Geometric model developed by Ratcliffe considered the effect of interconnectivity between filler particles [55]. Based on this existing geometric mean model, Agari and Uno [56] later established another model with the addition of new constants and successfully tested it with polymer composites. Moreover, Lewis and Nielsen proposed a model that considered the parameters of maximum packing number and volume fraction, as well as the effect of dispersed particles' orientation and shape [57,58].

In contrast, Cheng and Vachon employed a probabilistic model and assumed that the distributive function of the discontinuous phase between polymer matrix and filler particles was parabolic [59–61]. All these models are summarized in Table 3. Since certain factors, namely the effect of crystallinity, orientation of nanoparticles, or formation efficiency of conductive chains suggested in these historical models could not be readily quantified, the models that were selected for comparison with this work's experimental values for thermal conductivities were limited to the Geometric Mean, Maxwell and EMT models, respectively.

The various symbols in Table 1 corresponded to the following terms. K_c, K_{PCM} and K_F are the thermal conductivity of the composites, organic PCMs, and nanofiller respectively; $\varnothing$ is the volume fraction of the added nanofillers; $\varnothing_m$ is the maximum packing fraction of the dispersed particles; A is a constant that can be determined, depending on the orientation and shape of the dispersed nanoparticles; C_1 is a factor that influences the effect of crystallinity of the organic PCM matrix, and finally C_2 represents the ease in the formation of the conductive chains of the nanofiller particles.

The majority of the existing models presumed the PCM composite matrix to be filled with spherical or conic structures. However, nanoparticles such as GNPs and HBN could exhibit a flat and hexagonal thin-plate structure. Therefore, the current models would not be a good representation of the shape of the nanofillers. Instead, aspect ratios are better dimensional parameters to characterize the physical structures of the nanofillers, irrespective of their shapes.

Moreover, all the existing models have put emphasis on the thermal conductivity of the main polymer matrix. However, in reality, it was discovered that the major improvements in thermal conductivity were contributed mainly by the nanofillers, due to their much higher intrinsic thermal conductivities. Thus, a higher percentage share should be allocated to the thermal conductivity of the nanofillers. Furthermore, most of the existing models were tested using composites containing low loadings of filler particles, hence predictions for higher loadings were not accounted for. In addition, the presence of agglomerates of nanoparticles at large volumes can also lead to higher phonon scattering, hence hindering the phonons thermal paths. The PCM matrix might reach a saturation point where it cannot absorb any further nanofiller.

Based on the abovementioned limitations, a modified Maxwell model shown in Equation (4.1) is proposed in this study, to estimate the solid-state thermal conductivity of PCM composites at all loadings. By the trial-and-error of constant fitting, this new model replaced the intrinsic thermal conductivity of pristine PCM with the product of compatibility factor and aspect ratio.

$$K_{CPCM} = \frac{1}{A} \times C_{comp} \times \frac{K_F + 2K_{PCM} + 2\varnothing_f(K_F - K_{PCM})}{K_F + 2K_{PCM} - 2\varnothing_f(K_F - K_{PCM})} \tag{4.1}$$

where K_{CPCM} is the overall thermal conductivity of the PCM nanocomposite, K_{PCM} is the intrinsic thermal conductivity of the PCM matrix, $\varnothing_f$ is the volume fraction of the nanofillers, A is the aspect ratio of the nanofillers (which is better than the shape factor from previous models, as the majority of nanofillers are irregular in nature and will be structurally deformed upon intense mixing during the fabrication processes), K_F is the intrinsic thermal conductivity of the nanofillers, and C_{comp} is the compatibility factor for each composite, which will be derived from the experimental data. Each of these new suggested parameters for calculating the CPCM's thermal conductivity in this Maxwell-modified model are outlined in Table 4.

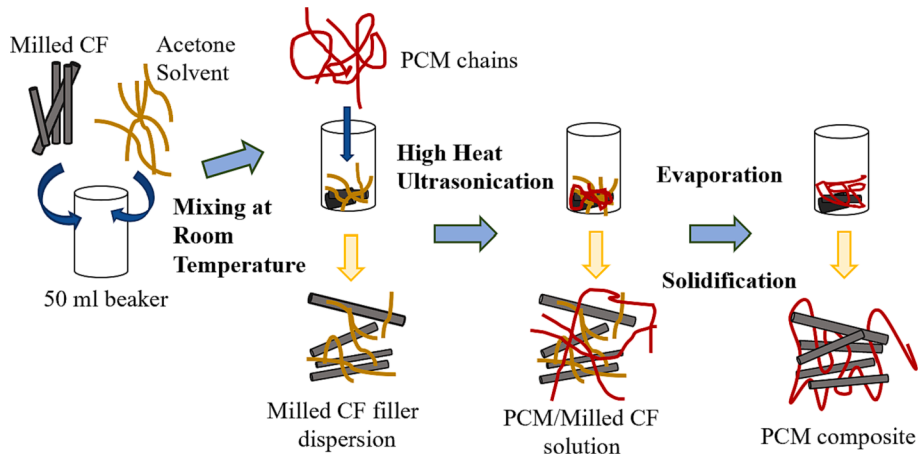

Fig. 1. The preparation steps for the temperature-assisted solution blending fabrication of MCF-incorporated PCM composites.

Table 3
A summary of the theoretical models on the thermal conductivity for composite materials.

Model Name	Model Formulae	Limitations of the Model
Maxwell [44]	$K_c = K_{PCM} \times \frac{K_F + 2K_{PCM} + 2\varnothing(K_F - K_{PCM})}{K_F + 2K_{PCM} - 2\varnothing(K_F - K_{PCM})}$	Invalid for large volume fractions of fillers (>25 wt%) and does not account for filler interactions.
EMT [54]	$K_c = \frac{1}{4}(\gamma + \sqrt{\gamma^2 + 8K_F K_{PCM}})$ $\gamma = (3\varnothing - 1)\times K_F + [3(1-\varnothing) - 1] \times K_{PCM}$	Invalid for high volume fractions of fillers (>25 wt%), requires samples of perfect inter-phases, and does not account for filler inter-connectivity at larger filler concentrations.
GeometricMean [55]	$K_c = {K_F}^{\varnothing} \times {K_M}^{1-\varnothing}$	Predictions only showed good agreement with experimental values from 0 wt% to 5 wt%.
Agari & Uno [56]	$logK_c = \varnothing C_2 logK_F + (1-\varnothing) log(C_1 K_{PCM})$	Predictions showed good agreement with experimental values for low filler loadings. Yet, it was difficult to measure the values of C1 and C2.
Lewis & Nielsen [57,58]	$K_c = K_{PCM} \times \frac{1 + A\left(\frac{\frac{K_F}{K_{PCM}} - 1}{\frac{K_F}{K_{PCM}} + A}\right)\varnothing}{1 - \varnothing\left(\frac{\frac{K_F}{K_{PCM}} - 1}{\frac{K_F}{K_{PCM}} + A}\right)\left(1 + \varnothing \times \frac{1 - \varnothing_m}{{\varnothing_m}^2}\right)}$	Despite a good agreement between experimental and predicted values, only a filler loading of up to 5 % were tested, and an average of filler loading of 3 % were used.
Cheng & Vachon [59–61]	$\frac{1}{K_c} = \frac{1-B}{K_{PCM}} + \frac{1}{\sqrt{C(K_F - K_{PCM})[K_{PCM} + B(K_F - K_{PCM})]}} \times ln\left[\frac{\sqrt{K_{PCM} + B(K_F - K_{PCM})} + \frac{B}{2}\sqrt{C(K_F - K_{PCM})}}{\sqrt{K_{PCM} + B(K_F - K_{PCM})} - \frac{B}{2}\sqrt{C(K_F - K_{PCM})}}\right]$ $where B = \left(\frac{3\varnothing}{2}\right)^{\frac{1}{2}}, C = \frac{4}{B}$	The model predicted the thermal conductivity best for suspensions, which were within 18.2 %. The effects of convection and radiant heat transfer as thermal mechanisms were not considered.

Table 4
A summary of all the new parameters in the Maxwell-revised model in this study, for the calculation of CPCM's thermal conductivity.

Symbol	Terminology	Units
A	aspect ratio of nanofillers	dimensionless
C_{comp}	compatibility factor of composite	dimensionless
K_F	thermal conductivity of filler	W m^{-1} K^{-1}
K_{PCM}	thermal conductivity of phase change material	W m^{-1} K^{-1}
K_{CPCM}	thermal conductivity of composite phase change material	W m^{-1} K^{-1}
$\varnothing_f$	volume fraction of nanofiller	dimensionless

The compatibility factor changes from one PCM to another, and it can also vary based on the purity and quality of the pristine PCMs. Thus, to derive a suitable value of C_{comp}, datasets for thermal conductivities and aspect ratios should be collected and, then, by starting at a reasonable value, be adjusted by increasing or decreasing the value of C_{comp} in MATLAB so that the slope of the plotted curves gradually fits with the predicted thermal conductivities.

This new model assumed that all the experimental measurements were carried out at temperatures between 290K and 300K, whereas it does not take into consideration the behavior of the PCM composites when there is significant agglomeration of particles, and it only predicts thermal conductivity values in the solid state. This is mainly due to the lack of data available for the liquid-state thermal conductivities for all organic PCM nanocomposites. To quantify the numerical comparisons between the experimental and empirical thermal conductivities, the normalized root-mean-square error (NRMSE) [62], calculated using Equation (4.2), was used.

$$NRMSE = \frac{1}{\sigma} \times \sqrt{\sum_{i=1}^{n} \frac{(\widehat{y}_i - y_i)^2}{n}} \tag{4.2}$$

where σ is the standard deviation of data points, n is the sample size, $\widehat{y}_i$ is the i th estimated value, and y_i is the i th actual value. Therefore, the lower the NRMSE, the smaller the mismatches between the measured and predicted thermal conductivities of the CPCMs will be.

4. Results and discussion

4.1. Structure and morphology of CPCMs

All the existing models for calculating the thermal conductivity of PCM composites assumed the base matrix to be filled with spherical or conic fillers. However, nanoparticles such as the MCFs employed in this study exhibited tubular structures with varying dimensions. The morphology of the PCM/MCF samples was analyzed using SEM. As shown by the SEM images in Fig. 2, the dispersity of the MCFs at low loadings (5 wt%) was quite uniform in both PCM matrices (i.e., paraffin and PEG), due to the weak Van der Waal's interactions between the MCF particles. Yet, the random alignment of the MCFs and their agglomerates at higher loadings (15 wt%) intensifies the phonon scattering, which reduces the speed of heat transfer. The shattered MCFs with shorter lengths that resulted from inconsistent manufacturing and intense ultrasonication, potentially led to obstructive channels for the heat carriers to flow through. In Fig. 2A and 2B, the paraffin/MCF composites exhibited progressively wrinkled surface textures with curling edges as the filler loading increased, and aggregation was observed at the highest loading (15 wt%) due to large specific surface areas and strong π–π bonding. Yet, the creases on these surfaces created network-like inter-filler structures which helped to enhance the matrix-filler interaction and accelerated the heat transfer through the composite.

Similarly, the overall surfaces appeared rougher in the PEG/MCF composites as the filler loading was increased, but fewer agglomerates were seen in this system. Spherulites were also observed in the pristine PEG, which accounted for its slightly higher thermal conductivity relative to that of pure paraffin. This is attributed to the fact that the PEG molecules with higher crystallinity have higher bond energies in their polymeric backbones, leading to enhanced thermal conductivity. However, some of the added MCFs were torn apart by the spherulites in the PEG matrices. This reduced the aspect ratio of the MCFs, which in turn decreased the intrinsic thermal properties of the MCFs, as well as the overall thermal conductivity of the composites. Moreover, Fig. 2C and 2F show that the surface of a single strand of MCF was very rough, with lots of indentations and unknown particles adhered to the fibrous structures and showing quite fussy cross-sectional outlines, which had an effect on the phonon–phonon and phonon-boundary scattering.

The chemical functional groups in the resulting paraffin/MCF and PEG/MCF samples were also investigated using the Fourier Transform Infrared Spectroscopy technique, as shown in Fig. 3. This was performed to assure that no chemical reactions took place within the mixing process, which might create new substances. In specific, the peaks present in paraffin wax corresponded to the typical long chain methyl CH_2 rocking, CH bending, and alkane (–C–H) stretch at wavenumbers 719 cm^{-1}, 1462 cm^{-1} and 2915 cm^{-1}, respectively, as seen in Fig. 3A. In addition, from Fig. 3B, the extra peaks observed in PEG were –C–O stretching and –O–H bending at wavenumbers 1095 cm^{-1} and 958 cm^{-1} respectively. Moreover, the characteristic peaks of strong C–C bonds at approximately 2900 cm^{-1} for milled CF were also significant in both types of composites. Hence, all these CPCMs contained the correct absorption peaks of the constituent raw materials. This confirmed that the milled CF was physically combined and incorporated to the pristine organic PCMs.

Nevertheless, the existing models, which only included the intrinsic thermal conductivities of pure PCMs and nanofillers, were not representative enough of the MCF-reinforced organic CPCMs, as the shape and smoothness of the MCF fillers, as well as their compatibility with the organic PCMs were not addressed. The aspect ratios were, thus, introduced in this new model to characterize the dimensions of MCFs, and the presence of nanoparticles' aggregates are also taken into consideration when estimating the overall thermal conductivity of these CPCMs.

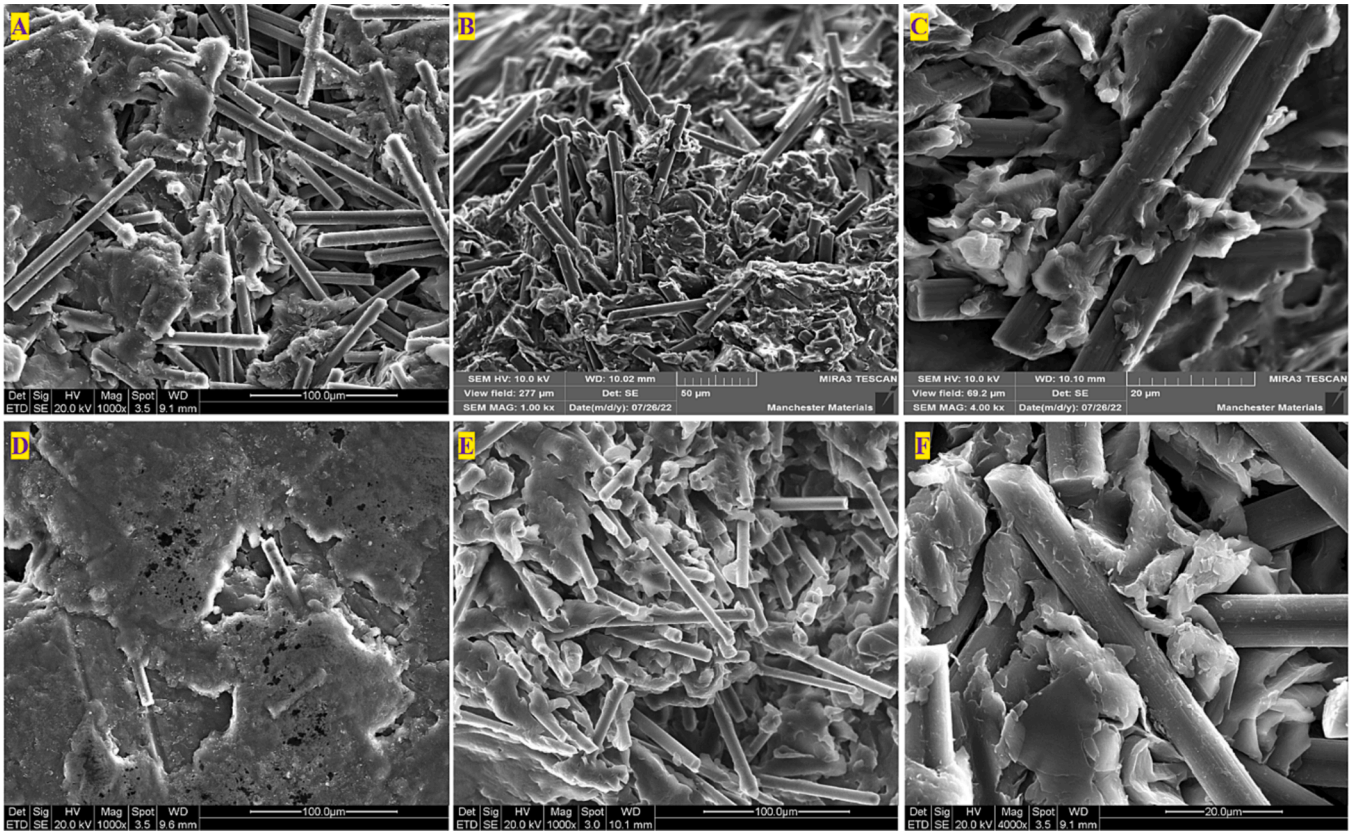

Fig. 2. SEM images of paraffin/MCF and PEG/MCF at 5 wt% (A, D) and 15 wt% (B, E) loading fractions respectively; as well as the SEM images of high magnification (4000X) of MCFs that were incorporated inside the paraffin (C) and PEG (F) matrices.

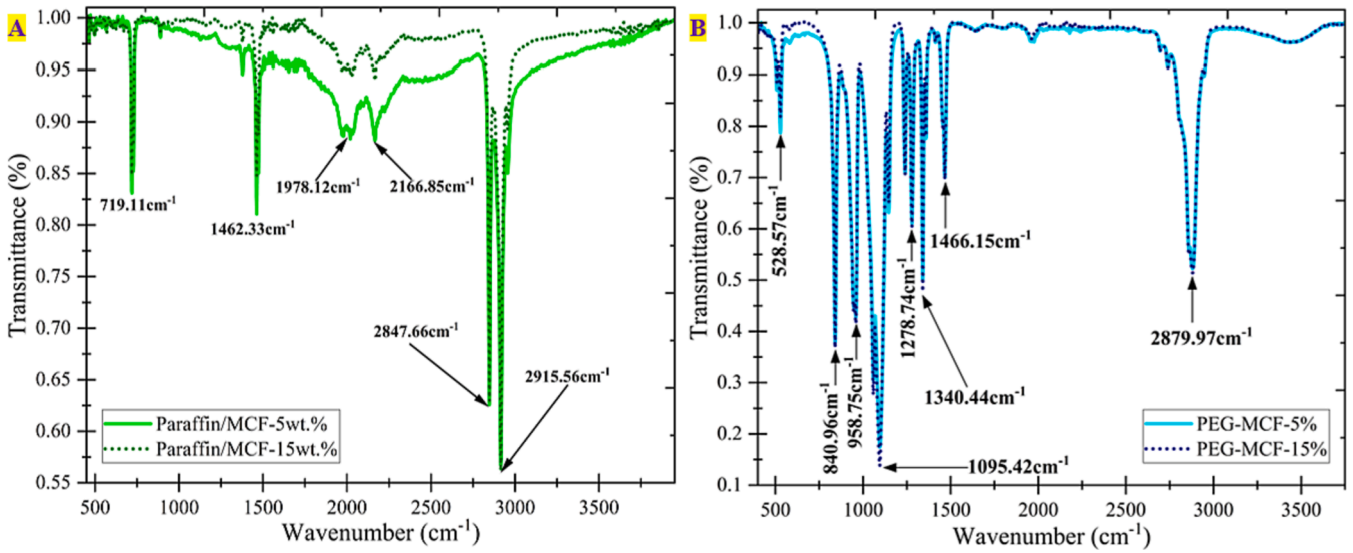

Fig. 3. The Fourier Transform Infrared Spectroscopy (FTIR) diagrams for paraffin/MCF (A) and PEG/MCF (B) composites at 5 wt% and 15 wt% loading fractions respectively.

4.3. Heat transfer properties of CPCMs

The thermal diffusivity and thermal conductivity of the paraffin/MCF and PEG/MCF composites, as shown in Fig. 4, were measured using a transient-line-sourced thermometer. It can be clearly seen that both properties increased progressively with MCF filler loadings in both systems. This finding was attributed to the fact that the intrinsic thermal conductivity of MCFs was much higher than that of neat paraffin and PEG. In Fig. 4A, the thermal diffusivity of paraffin/MCF was found to steadily increase from 0.26 $mm^2\ s^{-1}$ to 0.33 $mm^2\ s^{-1}$ with increasing filler loading, whereas the rate of growth was found to slightly decrease at filler loadings > 10 wt%. This was mainly attributed to the agglomeration of MCF particles, as these aggregates caused phonon scattering and deflected the heat carriers when they permeated the paraffin matrix [63]. Similarly, the thermal diffusivity of PEG/MCF reached a maximal value of 0.35 $mm^2\ s^{-1}$ at a filler loading of 15 wt%, as some of these MCF agglomerates oriented unidirectionally establishing a highly conductive channel that helps phonon diffusion, with the extent of improvement in the rate of heat transfer superseding the reverse impact of phonon interferences [64].

In Fig. 4B, the thermal conductivity of PEG/MCF also exhibited a linear rise of 56.4 % in the thermal conductivity from 0.294 $W\ m^{-1}\ K^{-1}$ to 0.673 $W\ m^{-1}\ K^{-1}$ with increasing filler loading. This implied that the spherulites present in the PEG matrix forced the MCF fillers to align in a particular direction, which promoted the flow of phonons in a single line of interest which, in turn, lowered the interfacial thermal contact resistance between the PEG matrix and the MCFs. Likewise, the thermal conductivity of paraffin/MCF also experienced a 57.1 % increment from 0.265 $W\ m^{-1}\ K^{-1}$ to 0.618 $W\ m^{-1}\ K^{-1}$ when the filler loading increased from 0 wt% to 16 wt%, reflecting that MCFs were equally compatible with the paraffin molecules. However, the thermal conductivity found for the paraffin/MCF was lower than that found for PEG/MCF, mainly due to the slightly lower intrinsic thermal conductivity of the paraffin relative to that of the PEG.

To further comprehend the thermal properties of MCF-incorporated CPCMs, in terms of storage applications, the melting temperature and enthalpies of fusion for paraffin/MCF and PEG/MCF composites were analysed, as shown in Fig. 5. The phase transition temperature, in Fig. 5A, from solid to liquid state, fluctuated between 55℃ and 59℃ for all both types of samples. In general, the PEG/MCF had slightly higher melting

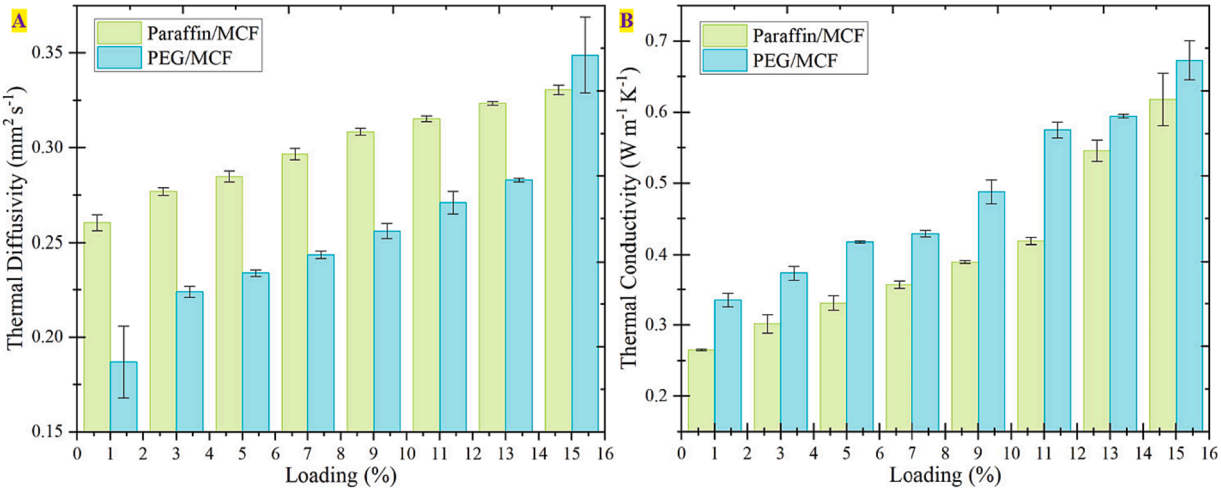

Fig. 4. The experimentally measured (A) thermal diffusivity and (B) thermal conductivity of paraffin/MCF and PEG/MCF composites.

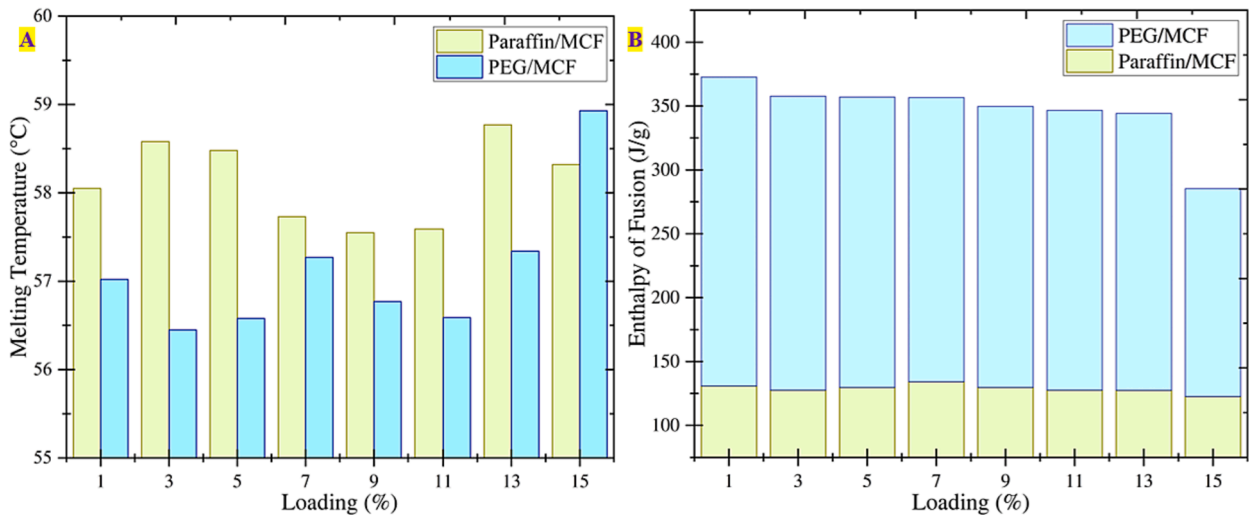

Fig. 5. The variation in melting temperature (A) and enthalpy of fusion (B) for paraffin/MCF and PEG/MCF composites as the loading fraction of fillers increased from 1 wt% to 15 wt%.

points than that of paraffin/MCF across different loadings, which can be attributed to the higher phase transition temperature of pristine PEG. Interestingly, there was no significant correlation between the melting temperature and the MCF loading. This meant that the intrinsic phase transition of pristine organic PCM were negligibly affected as the concentration of nanofillers was increased from 1 wt% to 15 wt%.

On the other hand, the overall enthalpy of fusion for both paraffin/MCF and PEG/MCF samples was inversely proportional to the nanofiller

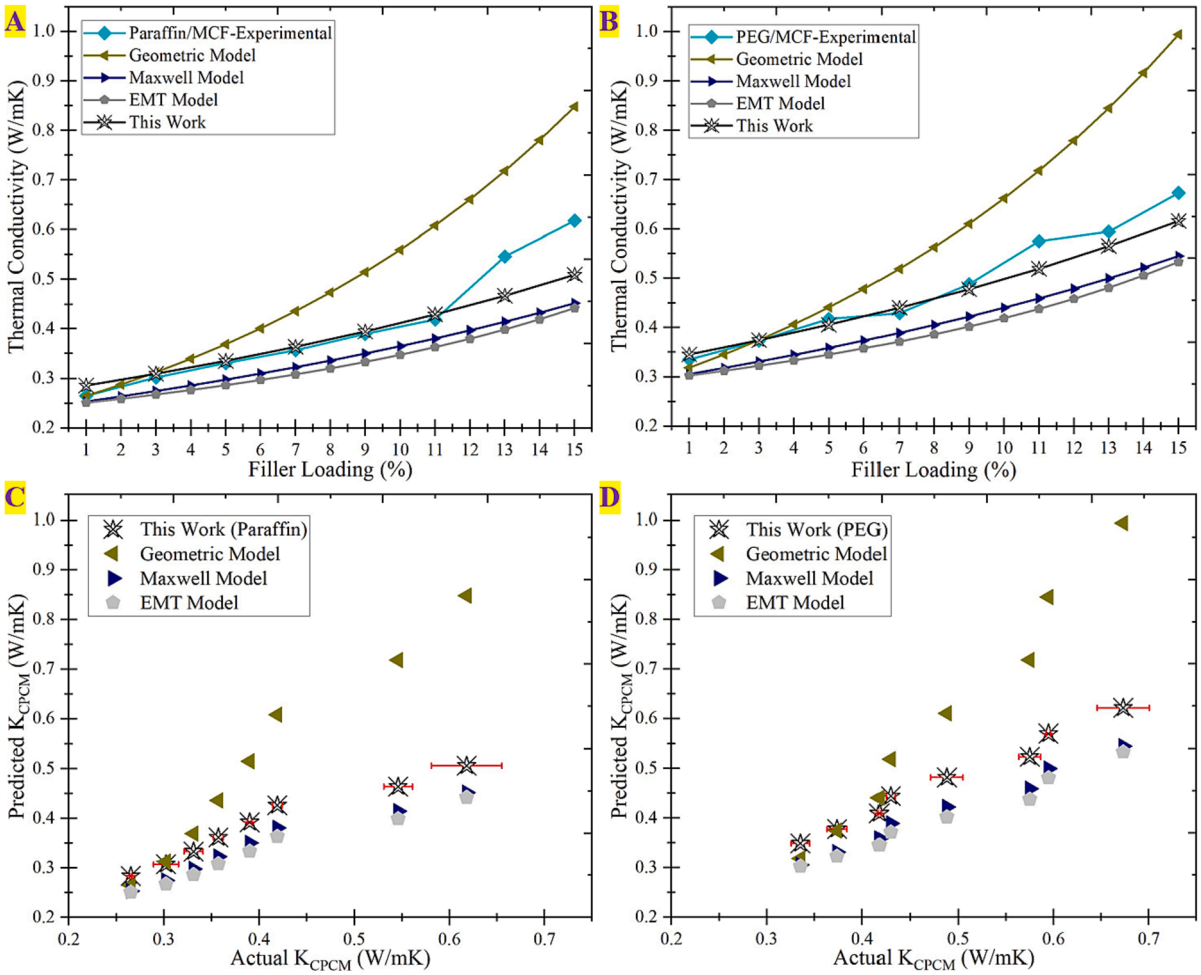

Fig. 6. A comparison of the existing theoretical models on the thermal conductivity of (A) paraffin/MCF and (B) PEG/MCF composites with this study's experimental values and the forecasted values from the modified Maxwell model as the MCF filler loadings increased from 1 wt% to 15 wt%, as well as two scatter plots illustrating the actual and predicted thermal conductivities for (C) paraffin/MCF and (D) PEG/MCF composites respectively.

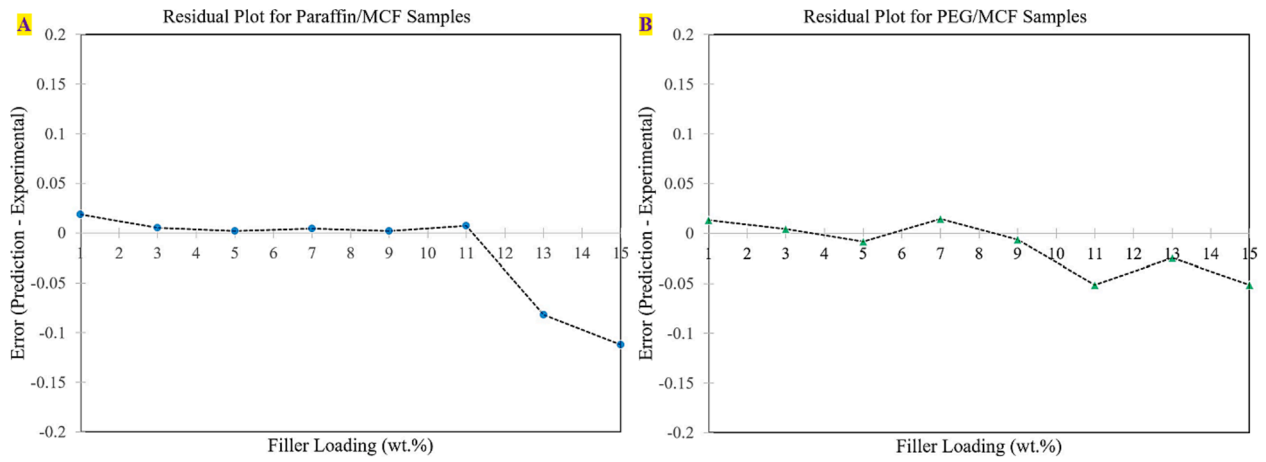

Fig. 7. Graphs illustrating the residuals calculated from the differences between the model predictions and actual experimental values for A) paraffin/MCF and B) PEG/MCF composites.

Table 5
Performance evaluation of the modified Maxwell model for different CPCMs.

	R^2 value	Normalized *RMSE*
Paraffin/MCF samples	0.983	0.123
PEG/MCF samples	0.996	0.058

loading, as shown in Fig. 5B. This is mainly the consequence of lower intrinsic latent heats for MCF fillers as compared to that of pristine PCM materials. Hence, as these MCFs take up much more space within the PCM matrices, there will be an increase in the pressure of the PCM pores, this decreases the molecular heat transfer and hence the enthalpy of fusion will decrease. Similar to that of melting temperature trends, all the PEG/MCF composites had a higher enthalpy of fusion than that of paraffin/MCF composites. This can be attributed to the higher intrinsic enthalpy of fusion of PEG in comparison with paraffin wax. From Fig. 5B, it can be observed that the paraffin/MCF samples experienced a very small increment of 2.53 % in enthalpies at lower MCF loadings (below 7 wt%). Due to the introduction of low amounts of MCFs, there was an increase in the degree of order in the molecule and increases the entropy of the system. Therefore, these MCFs formed interactions with the paraffin matrix and hence facilitated the network structure of the CPCMs, as a result it required more thermal energy to change the state from solid to liquid.

To summarize, the differences in the polymeric arrangements and trends in both systems implied that MCFs held better interactions with the PEG. After obtaining the thermometer-measured values of thermal conductivities of the CPCMs at various MCF filler loadings, these experimental data could then be compared with the predictions of the existing theoretical models and also used to justify the modified Maxwell model suggested in this study.

4.3. Validation of the modified Maxwell model

A comparative plot of the experimental thermal conductivities with those predicted using various models is displayed in Fig. 6. An aspect ratio of 13.3 was calculated for MCFs from the dimensions provided by the manufacturer whereas the measured intrinsic thermal conductivity of MCFs was approximately 1000 W m^{-1} K^{-1}. One drawback of this model was that any broken MCFs, which could reduce their aspect ratio, was not taken into account. From Fig. 6, it can be seen that the paraffin/MCF and PEG/MCF composites showed a better fit with this new model relative to previous models (which are Geometric Mean, Maxwell and EMT respectively), which must be mainly attributed to the inclusion of the aspect ratio and the compatibility factors. These parameters were not taken into account in the other models.

The compatibility factors, C_{comp}, trialed from MATLAB, were determined to be 3.625 and 4.455 for paraffin/MCF and PEG/MCF samples, respectively, and were in agreement with the thermal behavior found experimentally for these two systems. This implied that the PEG molecules were more compatible with the MCFs relative to the paraffin wax. The values for C_{comp} considered the differences between the network structure of core PCM matrices, as well as the nature of the interactions between the MCF fillers and these matrices. C_{comp} would also vary based on fabrication procedures and types of paraffin or PEG, such as shorter or longer chains of alkanes.

In terms of the effect of the volume fraction and aspect ratio of the nanofillers on the overall thermal conductivity of CPCMs, it was found that by minimizing the aspect ratio of the nanofillers, the thermal conductivity of CPCMs was improved. This finding was attributed to the suppression of large agglomerates of nanomaterials in the matrix, especially when long strands of MCF are used, such as in the present study. With regard to the volume fraction of the nanofillers, a substantial enhancement in the thermal conductivity of the CPCMs was observed with increasing volume fraction of highly-conductive nanofillers. However, depending on the type of pristine PCM, a very high loading of nanofiller particles can instigate some levels of aggregation, which will inhibit the flow of heat carriers, eventually leading to a saturation of the maximum thermal conductivity of the CPCMs.

Moreover, the agglomeration of the MCF particles that occurred at high loadings was found to deviate the thermal conductivity of the CPCMs. It could either 1) form a highly thermally conductive pathway that significantly improves the overall thermal conductivity, which can be modeled using exponentials or high-order polynomials, or 2) restrict the heat carriers and decrease the thermal conductivity, which can be alternatively modeled with logarithms or negatively-sloped linear polynomials.

From the residual plots shown in Fig. 7, it is clear that the thermal conductivities calculated for both CPCM systems had minimal differences from the experimental values. It can also be seen that the forecasted thermal conductivity of the PEG/MCF samples had fewer mismatches than that of the paraffin/MCF samples. This was further confirmed by the smaller normalized *RMSE* value of PEG/MCF relative to the paraffin/MCF, as displayed in Table 5. The half-lowered prediction errors determined for the PEG/MCF composites also reflected their better fit with the model, owing to the enhanced PEG/filler interactions and prominent compatibility relative to other system.

The presence of MCFs' aggregates at higher filler loadings usually interferes with the heat carriers, decreasing the rate of heat transfer,

although sometimes these agglomerated nanoparticles can establish a highly thermally conductive network, which then provides a continuous phase for the phonons to travel through. Regardless, at moderate filler loadings of approximately 10 wt%, the modified Maxwell model in this study exhibited an excellent fit to the experimental data for both CPCM systems, as confirmed by the R^2 values being extremely close to 1.

There are still a few limitations to this new model though. Firstly, this study is only valid for thermal conductivities of solid CPCMs, as it is difficult to accurately measure and model the thermal conductivities of liquid CPCMs. Secondly, this study was not able to account for potential aggregations of particles at high loadings. The tendency of the particles to agglomerate in the matrix depends on many factors, such as the quality of the raw PCMs, the composites fabrication methods, as well as the synthesis of the nanofillers. Besides, if cracks and voids were present in the samples, the predicted thermal conductivity of the CPCMs would also be accordingly reduced. All in all, this model will benefit from further justification with lots of different datasets.

5. Conclusions

In conclusion, to comprehend the heat transfer mechanisms of PCM/MCF composites, several factors must be taken into consideration, such as the dispersion of the MCF's in the matrix, the filler loading, the selection of the PCM matrix as well as the compatibility between the PCM matrix/MCF boundaries.

Hence, the modified Maxwell model suggested in this work estimated the thermal conductivity of paraffin/MCF and PEG/MCF composites quite accurately, in contrast to the previous models. Generally, as the phonon scattering increased due to the presence of agglomerates (especially at the high filler loadings), the thermal conduction pathways were adversely affected, which slowed down the diffusion rate of phonons, leading to reduced thermal diffusivity and thermal conductivity of the CPCMs. However, in special scenarios, these aggregates, when arranged in similar directions to the flow of phonons, could increase the rate of heat transfer. Despite the several breakthroughs, such as the much-improved thermal properties (due to the uniform distribution of MCF nanoparticles at moderate filler loadings), the research is still in its early stage as researchers attempted to address the bottlenecks of the precise estimation of CPCM's thermal conductivities. Some other factors that were not investigated in this study are:

1. The functionalization of the nanofillers to reduce the interfacial thermal contact resistance
2. The processing techniques for the nanofillers, such as using a magnetic field to promote an alignment of the MCFs in one direction to facilitate the phonon transfer through the matrix.
3. The porosity and viscosity of conventional PCMs in solid and liquid states

Therefore, this new model sheds light onto the prediction of the thermal conductivity of PCM/MCF composites and can be flexibly applied in CPCMs with different nanofillers and PCM matrices, as long as the aspect ratio of nanoparticles, intrinsic thermal conductivities of constituent materials, and the compatibility factors are individually assessed.

6. Notes

We would like to acknowledge the funding support provided by the Engineering and Physical Sciences Research Council (EPSRC), United Kingdom, under the grant number EP/T517823/1.

CRediT authorship contribution statement

Tan Lo Wong: Writing – review & editing, Writing – original draft, Visualization, Validation, Software, Resources, Project administration, Methodology, Investigation, Formal analysis, Data curation, Conceptualization. **Yasith S. Perera:** Software, Methodology, Funding acquisition. **Cristina Vallés:** Writing – review & editing, Visualization, Supervision. **Adel Nasser:** Writing – review & editing, Visualization, Supervision. **Chamil Abeykoon:** Writing – review & editing, Visualization, Supervision, Project administration, Funding acquisition.

Declaration of competing interest

The authors declare that they have no known competing financial interests or personal relationships that could have appeared to influence the work reported in this paper.

Data availability

Data will be made available on request.

References

[1] M.R. Reddy, N. Nallusamy, A.B. Prasad, H.K. Reddy, Thermal energy storage system using phase change materials: constant heat source, J. Therm. Sci. 16 (4) (2012) 1097–1104, https://doi.org/10.2298/TSCI100520078R.
[2] B. Zalba, J.M. Marın, L.F. Cabeza, H. Mehling, Review on thermal energy storage with phase change: materials, heat transfer analysis and applications, Appl. Therm. Eng. 23 (3) (2003) 251–283, https://doi.org/10.1016/S1359-4311(02)00192-8.
[3] D. Aydin, S.P. Casey, S. Riffat, The latest advancements on thermochemical heat storage systems, Renew. Sustain. Energy Rev. 41 (2015) 356–367, https://doi.org/10.1016/j.rser.2014.08.054.
[4] M. Liu, W. Saman, F. Bruno, Review on storage materials and thermal performance enhancement techniques for high-temperature phase change thermal storage systems, Renew. Sustain. Energy Rev. 16 (4) (2012) 2118–2132, https://doi.org/10.1016/j.rser.2012.01.020.
[5] S.S. Chandel, T. Agarwal, Review of current state of research on enegy storage, toxicity, health hazards and commercialization of phase changing materials, Renew. Sustain. Energy Rev. 67 (2017) 581–596, https://doi.org/10.1016/j.rser.2016.09.070.
[6] Y. Zhou, S. Wu, Y. Ma, H. Zhang, X. Zeng, F. Wu, F. Liu, J.E. Ryu, Z. Guo, Recent advances in organic/composite phase change materials for energy storage, ES Energy & Environment 9 (12) (2020) 28–40, https://doi.org/10.30919/esee8c150.
[7] A. Kasaeian, L. Bahrami, F. Pourfayaz, E. Khodabandeh, W.M. Yan, Experimental studies on the applications of PCMs and nano PCMs in buildings: a critical review, Energ. Buildings 154 (2017) 96–112, https://doi.org/10.1016/j.enbuild.2017.08.037.
[8] Z. Khan, A. Ghafoor, A review of performance enhancement of PCM based latent heat storage system within the context of materials, thermal stability and compatibility, Energ. Conver. Manage. 115 (2016) 132–158, https://doi.org/10.1016/j.enconman.2016.02.045.
[9] J. Yang, L.S. Tang, L. Bai, R.Y. Bao, Z.Y. Liu, B.H. Xie, M.B. Yang, W. Yang, High-performance composite phase change materials for energy conversion based on macroscopically three-dimensional structural materials, Mater. Horiz. 6 (2) (2019) 250–273, https://doi.org/10.1039/C8MH01219A.
[10] V. Goel, A. Saxena, M. Kumar, A. Thakur, A. Sharma, V. Bianco, Potential of phase change materials and their effective use in solar thermal applications: a critical review, Appl. Therm. Eng. 119417 (2022), https://doi.org/10.1016/j.applthermaleng.2022.119417.
[11] Wong, T.L. Vallés, C., Nasser, A., Abeykoon C. (2023). Zhang, P., Xiao, X., Ma, Z.W. (2016). Effects of boron-nitride-based nanomaterials on the thermal properties of composite organic phase change materials: A state-of-the-art review. Renewable and Sustainable Energy Reviews, 187, 113730, DOI: https://doi.org/10.1016/j.rser.2023.113730.
[12] X. Chen, H. Gao, Z. Tang, W. Dong, A. Li, G. Wang, Optimization strategies of composite phase change materials for thermal energy storage, transfer, conversion and utilization, Energ. Environ. Sci. 13 (12) (2020) 4498–4535, https://doi.org/10.1039/D0EE01355B.
[13] T.L. Wong, C. Vallés, A. Nasser, C. Abeykoon, A critical experimental evaluation of hexagonal boron nitride, graphene oxide and graphite as thermally conductive fillers in organic PCMs, J. Storage Mater. 72 (2023) 108523, https://doi.org/10.1016/j.est.2023.108523.
[14] D. Feng, Y. Feng, L. Qiu, P. Li, Y. Zang, H. Zou, Z. Yu, X. Zhang, Review on nanoporous composite phase change materials: fabrication, characterization, enhancement and molecular simulation, Renew. Sustain. Energy Rev. 109 (2019) 578–605, https://doi.org/10.1016/j.rser.2019.04.041.
[15] T.L. Wong, K. Ma, C. Abeykoon, Enhancing the thermal performance of polyethylene glycol phase change material with carbon-based fillers, International Journal of Mass and Heat Transfer 220 (2023) 124919, https://doi.org/10.1016/j.ijheatmasstransfer.2023.124919.
[16] Y. Huang, A. Stonehouse, C. Abeykoon, Encapsulation methods for phase change materials–a critical review, Int. J. Heat Mass Transf. 200 (2023) 123458, https://doi.org/10.1016/j.ijheatmasstransfer.2022.123458.

[17] A. Wazeer, A. Das, C. Abeykoon, A. Sinha, A. Karmakar, Phase change materials for battery thermal management of electric and hybrid vehicles: a review, Energy Nexus 100131 (2022), https://doi.org/10.1016/j.nexus.2022.100131.
[18] A. Stonehouse, C. Abeykoon, Thermal properties of phase change materials reinforced with multi-dimensional carbon nanomaterials, Int. J. Heat Mass Transf. 183 (2022) 122166, https://doi.org/10.1016/j.ijheatmasstransfer.2021.122166.
[19] A. Eitan, K. Jiang, D. Dukes, R. Andrews, L.S. Schadler, Surface modification of multiwalled carbon nanotubes: toward the tailoring of the interface in polymer composites, Chem. Mater. 15 (16) (2003) 3198–3201, https://doi.org/10.1021/cm020975d.
[20] A. Hirsch, Functionalization of single-walled carbon nanotubes, Angew. Chem. Int. Ed. 41 (11) (2022) 1853–1859, https://doi.org/10.1002/1521-3773(20020603)41:11<1853::AID-ANIE1853>3.0.CO;2-N.
[21] E. Hammel, X. Tang, M. Trampert, T. Schmitt, K. Mauthner, A. Eder, P. Pötschke, Carbon nanofibers for composite applications, Carbon 42 (5) (2014) 1153–1158, https://doi.org/10.1016/j.carbon.2003.12.043.
[22] L. Guadagno, M. Raimondo, V. Vittoria, L. Vertuccio, K. Lafdi, B. De Vivo, P. Lamberti, G. Spinelli, V. Tucci, The role of carbon nanofiber defects on the electrical and mechanical properties of CNF-based resins, Nanotechnology 24 (30) (2013) 305704, https://doi.org/10.1088/0957-4484/24/30/305704.
[23] K. Lafdi, W. Fox, M. Matzek, E. Yildiz, Effect of carbon nanofiber-matrix adhesion on polymeric nanocomposite properties-part II, J. Nanomater. (2008), https://doi.org/10.1155/2008/529890.
[24] K. Lafdi, W. Fox, M. Matzek, E. Yildiz, Effect of carbon nanofiber heat treatment on physical properties of polymeric nanocomposites—part I, J. Nanomater. (2007), https://doi.org/10.1155/2007/52729.
[25] M. Endo, Y.A. Kim, T. Hayashi, K. Nishimura, T. Matusita, K. Miyashita, M. S. Dresselhaus, Vapor-grown carbon fibers (VGCFs): basic properties and their battery applications, Carbon 39 (9) (2001) 1287–1297, https://doi.org/10.1016/S0008-6223(00)00295-5.
[26] M.H. Al-Saleh, U. Sundararaj, A review of vapor grown carbon nanofiber/polymer conductive composites, Carbon 47 (1) (2009) 2–22, https://doi.org/10.1016/j.carbon.2008.09.039.
[27] Y. Zhou, F. Pervin, S. Jeelani, Effect vapor grown carbon nanofiber on thermal and mechanical properties of epoxy, J. Mater. Sci. 42 (17) (2007) 7544–7553, https://doi.org/10.1007/s10853-007-1618-6.
[28] T. Uchida, D.P. Anderson, M.L. Minus, S. Kumar, Morphology and modulus of vapor grown carbon nano fibers, J. Mater. Sci. 41 (18) (2006) 5851–5856, https://doi.org/10.1007/s10853-006-0324-0.
[29] E. Mayhew, V. Prakash, Thermal conductivity of individual carbon nanofibers, Carbon 62 (2013) 493–500, https://doi.org/10.1016/j.carbon.2013.06.048.
[30] Easycomposites.co.uk. (2022). Milled Carbon Fibre Powder - Easy Composites. [online] Available at: <https://www.easycomposites.co.uk/milled-carbon-fibre-powder> [Accessed 10 December 2022].
[31] Y. Cui, C. Liu, S. Hu, X. Yu, The experimental exploration of carbon nanofiber and carbon nanotube additives on thermal behavior of phase change materials, Sol. Energy Mater. Sol. Cells 95 (4) (2011) 1208–1212, https://doi.org/10.1016/j.solmat.2011.01.021.
[32] J. Fukai, M. Kanou, Y. Kodama, O. Miyatake, Thermal conductivity enhancement of energy storage media using carbon fibers, Energ. Conver. Manage. 41 (14) (2000) 1543–1556, https://doi.org/10.1016/S0196-8904(99)00166-1.
[33] Z. Liu, H. Wei, B. Tang, S. Xu, Z. Shufen, Novel light–driven CF/PEG/SiO2 composite phase change materials with high thermal conductivity, Sol. Energy Mater. Sol. Cells 174 (2018) 538–544, https://doi.org/10.1016/j.solmat.2017.09.045.
[34] J.C.M. Garnett, Colours in metal glasses and in metallic films, Philos. Trans. R. Soc. Lond. A 203 (1904) 385–420, https://doi.org/10.1098/rsta.1904.0024.
[35] J. Maxwell, Clerk, Clarendon Press, A Treatise on Electricity and Magnetism, 1904.
[36] C.W. Nan, Physics of inhomogeneous inorganic materials, Prog. Mater Sci. 37 (1) (1993) 1–116, https://doi.org/10.1016/0079-6425(93)90004-5.
[37] H. Fricke, The Maxwell-Wagner dispersion in a suspension of ellipsoids, J. Phys. Chem. 57 (9) (1953) 934–937, https://doi.org/10.1021/j150510a018.
[38] D.P.H. Hasselman, L.F. Johnson, Effective thermal conductivity of composites with interfacial thermal barrier resistance, J. Compos. Mater. 21 (6) (1987) 508–515, https://doi.org/10.1177/002199838702100602.
[39] D.A.G. Bruggeman, The calculation of various physical constants of heterogeneous substances. I. the dielectric constants and conductivities of mixtures composed of isotropic substances, Ann. Phys. 416 (1935) 636–791, https://doi.org/10.1002/andp.19354160705.
[40] T.H.S. Sup, Dielectric properties of emulsions, Colloid Polym. Sci. 177 (1) (1961) 57–61.
[41] A.G. Every, Y. Tzou, D.P.H. Hasselman, R. Raj, The effect of particle size on the thermal conductivity of ZnS/diamond composites, Acta Metall. Mater. 40 (1) (1992) 123–129, https://doi.org/10.1016/0956-7151(92)90205-S.
[42] R. Landauer, The electrical resistance of binary metallic mixtures, J. Appl. Phys. 23 (7) (1952) 779–784, https://doi.org/10.1063/1.1702301.
[43] M. Wang, N. Pan, Predictions of effective physical properties of complex multiphase materials, Mater. Sci. Eng. R. Rep. 63 (1) (2008) 1–30, https://doi.org/10.1016/j.mser.2008.07.001.
[44] C.W. Nan, R. Birringer, D.R. Clarke, H. Gleiter, Effective thermal conductivity of particulate composites with interfacial thermal resistance, J. Appl. Phys. 81 (10) (1997) 6692–6699, https://doi.org/10.1063/1.365209.
[45] Z. Hashin, S. Shtrikman, A variational approach to the theory of the effective magnetic permeability of multiphase materials, J. Appl. Phys. 33 (10) (1962) 3125–3131, https://doi.org/10.1063/1.1728579.
[46] T. Mori, K. Tanaka, Average stress in matrix and average elastic energy of materials with misfitting inclusions, Acta Metall. 21 (5) (1973) 571–574, https://doi.org/10.1016/0001-6160(73)90064-3.
[47] Y. Benveniste, Effective thermal conductivity of composites with a thermal contact resistance between the constituents: nondilute case, J. Appl. Phys. 61 (8) (1987) 2840–2843, https://doi.org/10.1063/1.337877.
[48] K. Pietrak, T.S. Wiśniewski, A review of models for effective thermal conductivity of composite materials, Retrieved from, Journal of Power Technologies 95 (1) (2015) 14–24, https://www.papers.itc.pw.edu.pl/index.php/JPT/article/view/463.
[49] N. Burger, A. Laachachi, M. Ferriol, M. Lutz, V. Toniazzo, D. Ruch, Review of thermal conductivity in composites: mechanisms, parameters and theory, Prog. Polym. Sci. 61 (2016) 1–28, https://doi.org/10.1016/j.progpolymsci.2016.05.001.
[50] J.Z. Xu, B.Z. Gao, F.Y. Kang, A reconstruction of Maxwell model for effective thermal conductivity of composite materials, Appl. Therm. Eng. 102 (2016) 972–979, https://doi.org/10.1016/j.applthermaleng.2016.03.155.
[51] H.S. Kim, J.U. Jang, J. Yu, S.Y. Kim, Thermal conductivity of polymer composites based on the length of multi-walled carbon nanotubes, Compos. B Eng. 79 (2015) 505–512, https://doi.org/10.1016/j.compositesb.2015.05.012.
[52] S. Zhai, P. Zhang, Y. Xian, J. Zeng, B. Shi, Effective thermal conductivity of polymer composites: theoretical models and simulation models, Int. J. Heat Mass Transf. 117 (2018) 358–374, https://doi.org/10.1016/j.ijheatmasstransfer.2017.09.067.
[53] W.B. Zhang, Z.X. Zhang, J.H. Yang, T. Huang, N. Zhang, X.T. Zheng, Y. Wang, Z. W. Zhou, Largely enhanced thermal conductivity of poly (vinylidene fluoride)/carbon nanotube composites achieved by adding graphene oxide, Carbon 90 (2015) 242–254, https://doi.org/10.1016/j.carbon.2015.04.040.
[54] C.W. Nan, G. Liu, Y. Lin, M. Li, Interface effect on thermal conductivity of carbon nanotube composites, Appl. Phys. Lett. 85 (16) (2004) 3549–3551, https://doi.org/10.1063/1.1808874.
[55] W.M.J.H. Woodside, J.H. Messmer, Thermal conductivity of porous media. I. Unconsolidated sands, J. Appl. Phys. 32 (9) (1961) 1688–1699, https://doi.org/10.1063/1.1728419.
[56] Y. Zhang, Y. Xu, E. Suhir, Effect of rapid thermal annealing (RTA) on thermal properties of carbon nanofibre (CNF) arrays, J. Phys. D Appl. Phys. 39 (22) (2006) 4878, https://doi.org/10.1088/0022-3727/39/22/021.
[57] L.E. Nielsen, The thermal and electrical conductivity of two-phase systems, Ind. Eng. Chem. Fundam. 13 (1) (1974) 17–20, https://doi.org/10.1021/i160049a004.
[58] Y. Agari, A. Ueda, S. Nagai, Thermal conductivity of a polymer composite, J. Appl. Polym. Sci. 49 (9) (1993) 1625–1634, https://doi.org/10.1002/app.1993.070490914.
[59] S.C. Cheng, R.I. Vachon, The prediction of the thermal conductivity of two and three phase solid heterogeneous mixtures, Int. J. Heat Mass Transf. 12 (3) (1969) 249–264, https://doi.org/10.1016/0017-9310(69)90009-X.
[60] S. Okamoto, H. Ishida, A new theoretical equation for thermal conductivity of two-phase systems, J. Appl. Polym. Sci. 72 (13) (1999) 1689–1697, https://doi.org/10.1002/(SICI)1097-4628(19990624)72:13<1689::AID-APP5>3.0.CO;2-D.
[61] R.C. Progelhof, J.L. Throne, R.R. Ruetsch, Methods for predicting the thermal conductivity of composite systems: a review, Polym. Eng. Sci. 16 (9) (1976) 615–625, https://doi.org/10.1002/pen.760160905.
[62] Ostle, B. (1963). Statistics in research. *Statistics in research.*, (2nd Ed).
[63] J.N. Shi, M.D. Ger, Y.M. Liu, Y.C. Fan, N.T. Wen, C.K. Lin, N.W. Pu, Improving the thermal conductivity and shape-stabilization of phase change materials using nanographite additives, Carbon 51 (2013) 365–372, https://doi.org/10.1016/j.carbon.2012.08.068.
[64] S. Harish, D. Orejon, Y. Takata, M. Kohno, Thermal conductivity enhancement of lauric acid phase change nanocomposite with graphene nanoplatelets, Appl. Therm. Eng. 80 (2015) 205–211, https://doi.org/10.1016/j.applthermaleng.2015.01.056.